Published in final edited form as:
Mol Biosyst. 2013 June 7; 9(6): 1522–1534. doi:10.1039/c3mb25598k.

Salmonella Modulates Metabolism during Growth under Conditions that Induce Expression of Virulence Genes

Young-Mo Kim[1,#], **Brian J. Schmidt**[2,#], **Afshan S. Kidwai**[3], **Marcus B. Jones**[4], **Brooke L. Deatherage Kaiser**[1], **Heather M. Brewer**[5], **Hugh D. Mitchell**[1], **Bernhard O. Palsson**[2], **Jason E. McDermott**[1], **Fred Heffron**[3], **Richard D. Smith**[1], **Scott N. Peterson**[4,6], **Charles Ansong**[1], **Daniel R. Hyduke**[2], **Thomas O. Metz**[1,*], and **Joshua N. Adkins**[1,*]

[1]Fundamental and Computational Sciences Directorate, Pacific Northwest National Laboratory, Richland, WA 99352

[2]Department of Bioengineering, University of California at San Diego, San Diego, CA 92093

[3]Department of Molecular Microbiology and Immunology, Oregon Health & Science University, Portland, OR 97239

[4]J. Craig Venter Institute, Rockville, MD 20850

[5]Environmental Molecular Sciences Laboratory, Pacific Northwest National Laboratory, Richland, WA 99352

Abstract

Salmonella enterica serovar Typhimurium (*S*. Typhimurium) is a facultative pathogen that uses complex mechanisms to invade and proliferate within mammalian host cells. To investigate possible contributions of metabolic processes to virulence in *S*. Typhimurium grown under conditions known to induce expression of virulence genes, we used a metabolomics-driven systems biology approach coupled with genome scale modeling. First, we identified distinct metabolite profiles associated with bacteria grown in either rich or virulence-inducing media and report the most comprehensive coverage of the *S.* Typhimurium metabolome to date. Second, we applied an omics-informed genome scale modeling analysis of the functional consequences of adaptive alterations in *S*. Typhimurium metabolism during growth under our conditions. Modeling efforts highlighted a decreased cellular capability to both produce and utilize intracellular amino acids during stationary phase culture in virulence conditions, despite significant abundance increases for these molecules as observed by our metabolomics measurements. Furthermore, analyses of omics data in the context of the metabolic model indicated rewiring of the metabolic network to support pathways associated with virulence. For example, cellular concentrations of polyamines were perturbed, as well as the predicted capacity for secretion and uptake.

INTRODUCTION

Salmonella enterica serovar Typhimurium (*S*. Typhimurium) is a highly infectious pathogenic bacterium that frequently causes outbreaks of severe gastrointestinal infection (i.e. enteritis *Salmonella*) that are geographically exacerbated via the rapid modern food transport systems.[1–3] Further, new difficult to treat, drug-resistant isolates are emerging.[4, 5]

[*]To whom correspondence should be addressed: Thomas O. Metz, Biological Sciences Division, Pacific Northwest National Laboratory, P.O. Box 999, MSIN K8-98, Richland, WA, USA, Tel.: (509) 371-6581; Fax: (509) 371-6555; thomas.metz@pnnl.gov. Joshua N. Adkins, Biological Sciences Division, Pacific Northwest National Laboratory, P.O. Box 999, MSIN K8-98, Richland, WA, USA, Tel.: (509) 371-6583; Fax: (509) 371-6546; joshua.Adkins@pnnl.gov.
[6]Current affiliation: Sanford-Burnam Medical Research Institute La Jolla, CA 92037
[#]These authors contributed equally to this work.

Therefore, understanding the mechanisms of pathogen invasion and proliferation within the hosts is critical to reduce health and economic impacts.[6]

Current understanding of *S.* Typhimurium pathogenesis is being augmented and refined using systems biology approaches[7, 8] namely whole genome mutagenesis,[9, 10] transcriptomics,[11–17] and proteomics,[18–24] which can provide global, integrated insight into pathogenesis and virulence. However, there are few reports to date of the application of metabolomics in the study of *S.* Typhimurium virulence.[25–27]

Collectively, metabolomics is a rapidly developing field devoted to identifying qualitative and quantitative differences in metabolites among biological samples.[28] However, these analyses have not yet been widely implemented in the study of pathogenic bacteria. With respect to *S.* Typhimurium, there are five reports of metabolomics analyses of intracellular or volatile metabolites in the context of biofilm formation[25] or as a potential diagnostic tool for determining food spoilage[29–31] or bacterial infection.[32] Thus, analyses of changes in metabolite profiles of *S.* Typhimurium during growth in virulence inducing conditions is timely, particularly as complementary systems biology (e.g., transcriptomics and proteomics) data sets from the same growth conditions are available to integrate with or assist in the analysis of metabolomics data.

A unique benefit of systems biology approaches is the ability to utilize relatively comprehensive datasets to globally inform predictions made using genome-scale metabolic models.[33] For example, model-guided analysis of time-series microarray data from *Pseudomonas aeruginosa* isolated from a cystic fibrosis patient yielded insight into tradeoffs between virulence factor and biofilm production during infection.[34] Global models of *S.* Typhimurium metabolism have been developed,[35–37] yielding a better understanding of gene essentiality and resulting in the identification of potential drug targets. However, an in-depth analysis utilizing them as a framework to integrate multi-omics data sets to gain a better understanding of metabolic processes during in vitro virulence conditions has not been performed. This is especially valuable where metabolomics analysis of pathogens isolated from host cells can be challenging due to the broad dynamic range of metabolite concentrations and the inability to distinguish host from pathogen metabolites.

We therefore performed intracellular metabolomics analyses of *S.* Typhimurium grown in both a rich medium and a minimal medium that induces the expression of virulence genes,[38, 39] including those on pathogenicity islands 1 and 2 (SPI-1 and SPI-2, respectively), which are responsible for encoding two type III secretion systems that deliver effector proteins essential for virulence SPI-1 is induced by growth in rich medium and is required for intestinal infection, while SPI-2 is induced in minimal acidic medium and is required for systemic infection. The resulting data were interpreted in the context of a constraints-based metabolic model of *S.* Typhimurium to evaluate metabolic changes associated with the induction of the virulence program.[18, 19, 40, 41]

Model-guided data analysis suggested fewer nutritional dependencies for maintaining optimal growth in virulence conditions, which may help to counter host nutrient sequestering strategies. Intriguingly, metabolites that were recently associated with immunoactivation and immunosuppression of macrophages[42] were identified in the current study as differentially abundant. Our results suggest that production and consumption of these putative ‘immunomodulatory’ metabolites may be regulated by the pathogen. Finally, following entry into stationary phase in virulence conditions, an increase in the intracellular abundances of amino acids is observed in *S.* Typhimurium. A model-guided analysis of matching transcriptomics data from analysis of cells grown in virulence-inducing media

suggests *S.* Typhimurium de-emphasizes these pathways and prioritizes other subsystems important to virulence, including lipopolysaccharide (LPS) and fatty acid biosynthesis.

MATERIALS AND METHODS

Chemicals and materials

All chemicals and reagents were purchased from Sigma-Aldrich (St. Louis, MO) unless otherwise noted. 3,5-Dibromotyrosine was purchased from Tokyo Chemical Industry (Tokyo, Japan) and used as an internal standard. Ammonium bicarbonate was purchased from Merck (Darmstadt, Germany), while a mixture of fatty acid methyl esters (FAMEs) and deuterated myristic acid were obtained from Agilent Technologies, Inc (Santa Clara, CA). Zirconium/silica beads (0.1 mm) were purchased from Biospec Products (Bartlesville, OK) and used for cell lysis. Deionized and purified water was used to prepare buffer and standard solutions (Nanopure Infinity ultrapure water system, Barnstead, Newton, WA).

Sample preparation

S. Typhimurium wild type cells (ATCC 14028) were used throughout this study and were taken from a single colony on an agar plate, subsequently inoculated into 7 mL of Luria-Bertani (LB) media (comprised of 1% tryptone, 0.5% yeast extract, and 1% sodium chloride at pH 7), and incubated overnight at 37°C. The overnight culture was centrifuged and the supernatant discarded. The cell pellets were suspended in LB media and centrifuged again, and the supernatant was discarded. For LB cultures, the cell pellets were subsequently suspended in 2 mL of LB media and used to inoculate 700 mL of LB in a 2.8 L flask. After 160 min of growth, cells were harvested via centrifugation (4,000×g) and washed twice with Dulbecco's PBS (Mediatech) once cultures reached an OD_{600} of +1.0.

To stimulate the *Salmonella* virulence program, cells were transferred to a low pH, low magnesium, and low iron (LPM) medium comprised of 8 μM $MgCL_2$, 0.5 μM ferric citrate, 5 mM KCl, 7.5 mM NH_4SO_4, 0.5 mM K_2SO_4, 0.3% glycerol v/v, 0.00001% thiamine, 337 μM H_3PO_4, and 80 mM 2-(*N*-morpholino)ethanesulfonic acid at pH 5.8.[38, 39] Briefly, cell pellets from the 7 mL LB media were suspended in LPM media and centrifuged. The supernatant was discarded and cell pellets were suspended in 2 mL of LPM media and used to inoculate 700 mL of LPM in a 2.8 L flask. Cells were harvested after 4 h or 20 h, then washed and isolated as above.

Three biological replicates were performed for each of the conditions (Scheme 1) described above. Cell pellets were stored at −80°C prior to thawing and were subsequently resuspended in an appropriate volume of 100 mM ammonium bicarbonate according to their wet weight to compensate for any differences in cell numbers. The cells were lysed by bead-beating, and the lysates were transferred into new tubes. Subsequently, 100 μL aliquots of cell lysates were extracted with four volumes of chilled (−20°C) chloroform/methanol (2:1, v/v), and the aqueous phases after centrifugation were transferred to glass vials and dried *in vacuo* (SpeedVac; Thermo Scientific, Waltham, MA). All samples were kept at −80°C prior to chemical derivatization for GC-MS analysis.

Chemical derivatization of metabolites and GC-MS analysis

Dried metabolite extracts were briefly dried again to remove any residual water prior to chemical derivatization as previously described.[43] To protect carbonyl groups and reduce the number of tautomeric isomers, 20 μL of methoxyamine in pyridine (30 mg/mL) were added to each sample, followed by incubation at 37°C with generous shaking for 90 min. To derivatize hydroxyl and amine groups to trimethylsilyated (TMS) forms, 80 μL of *N*-methyl-*N*-(trimethylsilyl)trifluoroacetamide (MSTFA) with 1% trimethylchlorosilane

(TMCS) were then added to each vial, followed by incubation at 37°C with shaking for 30 min. The samples were allowed to cool to room temperature and were then analyzed by GC-MS in random order. For technical replicates, each of the derivatized samples was split into two different vials and analyzed separately.

An Agilent GC 7890A coupled with a single quadrupole MSD 5975C (Agilent Technologies, Inc) was used for all analyses, and separations were performed using a HP-5MS column (30 m × 0.25 mm × 0.25 μm; Agilent Technologies, Inc). The sample injection mode was splitless, and 1 μL of each sample was injected. The GC oven was held at 60°C for 1 min after injection, and the temperature was then increased to 325°C by 10°C/min, followed by a 5 min hold at 325°C.[44] The injection port temperature was held at 250°C throughout the analysis.

GC-MS data-processing and analysis

GC-MS raw data files were processed using MetaboliteDetector.[45] Retention indices (RI) of detected metabolites were calculated based on analyses of a mixture of FAMEs (C8 – C30), followed by their chromatographic alignment across all analyses after deconvolution. Metabolites were then identified by matching GC-MS features (characterized by measured retention indices and mass spectra) to the Agilent Fiehn Metabolomics Retention Time Locked (RTL) Library,[44] which contains spectra and validated retention indices for 700 metabolites. All metabolite identifications were manually validated to reduce deconvolution errors during automated data-processing and to eliminate false identifications. In addition, an occurrence filter was applied to remove those features that were detected in fewer than 6 out of 18 GC-MS analyses. The curated data matrix of identified metabolites, unidentified features, and their abundances for each sample was then loaded into DAnTE[46] for statistical analysis. Data were first converted to Log2 scale, followed by Pearson's correlation and principal component analyses (PCA) to assess the reproducibility of the experiment and to identify natural clustering within the data, respectively.

During the TMS derivatization of metabolites, partial derivatives having different numbers of TMS groups can be generated.[47] In these instances, the most abundant GC-MS peak for each metabolite was selected, or the integrated areas of two or three peaks were combined when those peaks had relatively similar abundances.

Microarray analysis

Condition-matched *S.* Typhimurium cultures were utilized for mRNA extraction at the J Craig Venter Institute (JCVI), and gene expression was quantified with JCVI *S.* Typhimurium 13k v8 two-channel spotted oligonucleotide microarrays. Data from 193 microarrays (75 replicates in LB, 70 replicates and 48 replicates from 4 and 20 h in LPM media, respectively) were extracted using the *limma* package for R from Bioconductor,[48] background-corrected with the normexp method,[49] normalized using the print-tip LOESS method, and adjusted by quantile normalization between the channels and arrays.

Data dissemination

All raw and processed metabolomics data will be made available via the Metabolights metabolomics data repository (http://www.ebi.ac.uk/metabolights/index). Raw metabolomics data will also be made available via the PNNL Biological MS Data and Software Distribution Center ((http://omics.pnl.gov/). Microarray data corresponding to wild type *Salmonella* in LB and LPM media, as well as various mutant strains, is available via the Gene Expression Omnibus (http://www.ncbi.nlm.nih.gov/geo/) under Series GSE25441. The previously published proteomics data referenced in the Discussion is available via the PNNL Biological MS Data and Software Distribution Center under accession number PNNL_1025.

Model-guided analysis of omics datasets

A genome-scale reconstruction of *S.* Typhimurium's metabolic network[35, 50] was employed for integrated analysis of omics datasets. Genome-scale reconstructions are biochemically, genetically, and genomically consistent knowledgebases that are amenable to conversion into mathematical models for functional and structural analyses.[51] Functional analysis refers to simulating cellular phenotypes, such as growth rates, and is often undertaken with flux balance analysis (see Orth et al. for a review of FBA[52]). Because genome-scale reconstructions employ a boolean formalism that relates genomic loci to enzymatic reactions they are increasingly used as a framework for analysis of various omics data types.[33] All simulations were performed with COBRA for Python[35, 50] (http://opencobra.sourceforge.net), unless otherwise specified.

We used transcriptomics and metabolomics data to construct condition-specific models for S. Typhimurium grown in LB and LPM at 4 h (LPM 4h). Transcriptomics data were integrated with the model using the GIMME algorithm, as previously described in Becker et al. [53]. In short, the GIMME algorithm seeks to minimize discrepancies between transcriptome data and the model pathways required to simulate a specified objective. Here, we used growth rate as the simulation objective for growth in LB and LPM 4h. It was not possible to perform flux balance analysis for the LPM 20 h samples because the culture had exited log-phase and there was no obvious simulation objective.

We devised an algorithm (described in Schmidt et al. in review) to incorporate the metabolomics data. In short, the algorithm requires that the condition-specific model is able to carry flux through at least one enzymatic reaction for each detected metabolite subject to the transcriptomic measurements and a simulation objective. Due to numerical limitations of most simulation software, it is important to note that reaction fluxes must be greater than the solver tolerance to be considered active. Here, simulated reaction fluxes needed to exceed the minimal tolerance (1×10^{-8}) for the ILOG/CPLEX to be considered non-zero.

To determine if the space of accessible metabolic fluxes differed for the LB versus the LPM 4h models, flux variability analysis was employed.[54] Flux variability analysis is a method that determines the allowable range of reaction flux for a specific model given the growth medium composition and a specified simulation objective. Alterations in flux ranges for reactions between conditions were characterized by the relative flux range change, defined as:

$$x = \frac{c_2 - c_1}{(r_2 - r_1)/2} \quad (1)$$

Here, c_i indicates the center of the flux range and r_i indicates the width of the flux range for condition i. A critical cutoff to employ when interpreting the change in flux is $|x| > 1$. If $x > 1$, the reaction in the first condition must carry more flux than in the second condition; i.e., the reaction is more active in the first condition. If $x < 1$, the reaction in the first condition must carry less flux than in the second condition; i.e., the reaction is less active in the first condition. When $0 < |x| < 1$, there is overlap in the flux ranges for the reactions across the conditions; i.e., the reactions may have the same activity.

In order to develop insights into the biological subsystems most impacted by the alterations in reaction flux, an enrichment analysis of the model reactions where $|x| > 1$, was performed. Subsystem data for model genes and metabolites were downloaded from KEGG[55, 56] and enrichment analysis was performed with Fisher's exact method and Benjamini and

Hochberg's false discovery rate correction in Gitools.[57] The KEGG "metabolic pathways" subsystem was filtered from the analysis.

In order to develop insight into metabolic alterations between the two LPM time points, we performed structural analyses of transcriptomics and metabolomics data with the model. Structural analysis refers to using the model as a 'graph' on which to organize the data to aid in identification of prominent features. Here, the model structure and the transcriptomics data were used to inform an analysis of reporter metabolites.[58, 59] The Reporter Metabolites algorithm identifies metabolites in a biochemical network that are associated with a significant number of differentially expressed genes. The lmscFit function from the *limma* package[48] for R[60] was employed to calculate p-values for alterations in gene expression, and integrated network diagrams of significant alterations were drawn in Cytoscape.[61]

Additionally, a qualitative analysis of alterations in subsystem prioritization was conducted. We constructed a condition-specific model for the LPM 20 h subject to the omics measurements and the ability to produce biomass. Next, we optimized the LPM 4 and 20 h models for the turnover of each metabolite in our GC-MS data set. Then we compared theses turnover capacities for LPM4 vs the LPM20. Metabolites were classified as exhibiting "increased," "maintained," or "reduced" priority based on how the qualitative analysis predicted the maxmimal turnover in LPM 20 vs 4 h. Subsystem enrichment analysis was also performed on the different classes of metabolites metabolites using model KEGG identifiers to gain insight into network alterations.

RESULTS

Overview of GC-MS-based S. Typhimurium metabolomics data

To identify metabolic changes associated with the expression of virulence genes, we performed metabolomics analyses of *S.* Typhimurium grown in LB and LPM media (Scheme 1), the latter of which has been shown to induce the expression of virulence genes.[38, 39] On average, 245 unique metabolite features (annotated with measured mass spectra and retention indices) were detected across 18 GC-MS analyses, and 124 of these were initially matched to entries in the Agilent Fiehn Metabolomics RTL Library. After manual validation of database matches (i.e., inspection of mass spectral and retention index matches), 66 metabolites were found to be confidently identified, representing the broadest coverage of the *S.* Typhimurium metabolome reported to date when compared to recent analyses of volatile[30, 32] or soluble[25, 29, 31] metabolites from this organism. A data matrix of identified metabolites and their abundances is provided as Supplemental Table S1. A representative GC-MS chromatogram is shown in Supplemental Figure S1. Pearson's correlation analysis of the curated data matrix (data not shown) indicated that data from instrumental replicates were highly correlated (>0.99), whereas data from biological replicates within treatment groups were less correlated (averages of 0.95–0.98).

Metabolome alterations induced by growth condition

The differences between growth conditions drove the segregation of data in a principal components analysis scores plot (Figure 1). To better visualize the similarities and differences between growth conditions, we constructed a heatmap of metabolite abundances for the 66 confidently identified metabolites (Figure 2). Each growth condition clearly shows differences in metabolite abundance as identified by GC-MS. Metabolites involved in glycerol catabolism, such as glycerol, glycerol 3-phosphate, dihydroxyacetone phosphate ($p = 1.8 \times 10^{-2}$), and pyruvate ($p = 2.3 \times 10^{-2}$), accumulated in *S.* Typhimurium grown in the rich LB medium but were depleted in cells upon the switch to LPM medium. In contrast, glucose was detected in relatively lower abundance in cells grown in LB relative to LPM

media. These observations are consistent with previous reports that glucose is the preferred carbon source of *S. Typhimurium* when available[62–64] and indicates flux through the glycerol catabolism pathway in LPM medium where glycerol is the sole carbon source. Metabolites comprising beta alanine metabolism –beta-alanine ($p = 1.7 \times 10^{-3}$), diaminopropane ($p = 9.9 \times 10^{-3}$), spermidine ($p = 9.4 \times 10^{-7}$), and malonate ($p = 1.4 \times 10^{-3}$) – were also increased in LB relative to LPM media. Malonate is a precursor in fatty acid biosynthesis, and various saturated (myristate) and mono-unsaturated fatty acids (oleate and palmitoleate, $p = 4.4 \times 10^{-3}$) were also more abundant in LB prior to the shift to LPM media. Amino acids appear to be consumed during log-phase growth in LB medium but dramatically increase in abundance upon the shift to LPM medium, particularly at 20 h (Figure 1). All metabolites with statistically significant differences in abundance between growth conditions as determined by t-test with Bonferroni correction[65] are shown in Table 1.

Model-guided analysis

To explore the systems level phenomena contributing to variations in the metabolome across growth media, we used our previously published genome-scale model of *S.* Typhimurium metabolism as a platform for multi-omics data analysis.[35] The model exhibited good coverage of the experimental observations – over 90% of the confidently identified metabolites mapped to the model (Table 2), while 1265 of 1270 genes represented in the model mapped to microarray data for *S.* Typhimurium grown in matched conditions.

Enrichment analysis of altered flux ranges

In order to characterize how *S.* Typhimurium adapts from growth in LB to LPM medium, we used metabolomics and transcriptomics data to construct condition-specific models. Then we identified reactions, and metabolite turnovers, with flux ranges that were exclusive to each condition-specific model (Supplemental Table S2). To identify underlying biological themes associated with these metabolites, we characterized the reactions and metabolites by subsystem enrichment analysis. In order to map the flux range results to impacted subsystems, we used the identities of genes encoding for enzymes governing reactions or KEGG compound identifiers for metabolites (Supplemental Tables S3 and S4).

KEGG pathway enrichment analysis of reactions with exclusive flux ranges ($|x| > 1$) identified differences in pyruvate metabolism, glycolysis/gluconeogenesis, methane metabolism, D-alanine metabolism, folate biosynthesis, D-glutamine and D-glutamate metabolism, and nitrogen metabolism. Supporting these findings, the abundances of pyruvate ($p = 2.6 \times 10^{-2}$), glucose-6-phosphate ($p = 8.5 \times 10^{-3}$), and L-alanine ($p = 5.1 \times 10^{-3}$) were significantly altered upon the shift from LB to LPM media (Table 2).

Similarly, model-guided analysis of metabolite turnover flux changes (LPM versus LB) resulted in the identification of changes in metabolites mapping to fatty acid biosynthesis, peptidoglycan biosynthesis, folate biosynthesis, methane metabolism, cysteine and methionine metabolism, glycolysis/gluconeogenesis, and nitrogen metabolism (Supplemental Table S4). These results illustrate broad differences in metabolic processes as *S.* Typhimurium adapts from growth in media rich in complex nutrients to an acidic environment with glycerol and ammonium as carbon and nitrogen sources, respectively.

Next, we performed a comparison of changes in the experimentally quantified intracellular metabolite abundances with changes in the previously described modeled metabolite turnover flux. Forty-three of the metabolites that were quantified in both growth conditions were present in the metabolic model and were not dead-ends nor present in thermodynamically infeasible loops[66, 67] (Figure 3A).

We have previously predicted that there are a number of metabolites whose production, or consumption, are implicated in macrophage activation.[42] Several predictions from our previous study were well-supported in the literature. For example, an increase in glucose oxidation in Bacillus Calmette–Guérin-activated macrophages has been reported to correspond with increases in hydrogen peroxide production in response to a number of additional stimuli, such as LPS.[68] Seventeen of these were detected by metabolomics (Supplemental Table S5). Experimentally quantified intracellular metabolites that were previously predicted to enhance macrophage activation[42] were preferentially increased in LPM relative to LB media (Figure 3B, $p = 1.5 \times 10^{-2}$, rank-sum permutation test, y-axis). Whereas, the turnover rates for immunostimulatory metabolites exhibited a preferential decrease in their allowable flux range (Figure 3B, $p = 6.0 \times 10^{-2}$, rank-sum permutation test, x-axis). Our analysis supports the hypothesis that even though many cellular metabolites with a putative propensity for macrophage activation increase with respect to intracellular concentration in LPM medium, their rate of production and consumption decreases. Because our measurements and predictions pertain to intracellular concentrations and fluxes, they do not necessarily reflect the external environment. It is plausible that *S.* Typhimurium could be sequestering immunostimulatory metabolites by decreasing export rates.

To investigate how *S.* Typhimurium's internal state may influence the external environment, we assessed the ability of the condition-specific models to consume and produce immunomodulatory amino acids, fatty acids, and polyamines (Figure 4). In LPM medium, the consumption of glycerol and ammonium were essential (not shown) and agrees well with the experimental observation of depletion of metabolites in the glycerol catabolism pathway (Figure 2). Glycerol and ammonium are the sole carbon and nitrogen sources, respectively, in LPM medium. Whereas, in LB medium the consumption of thirteen different metabolites (L-threonine, L-tryptophan, L-phenylalanine, L-methionine, L-tyrosine, L-leucine, L-serine, L-valine, L-lysine, L-histidine, L-arginine, L-glucose, and L-proline) was found to be essential for near optimal (99%) growth (Figure 2).

We have previously suggested that consumption of select "immunoinhibitory" metabolites by macrophages can reduce activation functions.[42] In short, the consumption of select metabolites by macrophages can inhibit or stimulate the macrophages capacity to produce NO, ATP, or NADH. In line with this suggestion, several inhibitory metabolites may be produced by *S.* Typhimurium in virulence conditions (Figure 4B). Interestingly, secretion of putrescine was also found to be essential for near optimal growth in a manner consistent with the omics-constraints in LB medium.

Analysis of Structural Changes in Log and Stationary Phase

The marked differences in metabolomic profiles as *S.* Typhimurium transitions from LB log to LPM log to LPM stationary phases (Figure 2 and Table 2) may be indicative of metabolic alterations that occur when *S.* Typhimurium exits the nutrient rich intestine and attempts to colonize hostile host cells. Entry into stationary phase was previously shown to induce additional *Salmonella* virulence genes and promote acid tolerance and resistence to oxidative stresses.[69, 70]

To identify metabolic changes associated with the transition from a rich environment to a poor environment and the exit to stationary phase, we performed reporter metabolites analysis[58] on the transcriptome data. The 10 metabolites associated with the most significant transcriptional perturbations are shown in Figure 5A and 5B for the transition from LB to LPM media at 4 h and for LPM medium from 4 to 20 h, respectively. Network maps illustrating the integration of significantly altered metabolites as quantified by GC-MS and the reporter method between LB and LPM at 4 h as well as LPM at 4 and 20 h are shown in Supplemental Figure S2 and S3, respectively.

Despite the experimentally observed large alterations in cellular amino acid concentrations between 4 and 20 h (Figure 1), amino acids did not score among the metabolites with the most significant alterations in related transcripts by the reporter metabolite analysis (Figure 5B). Instead, the most significant changes in the reporter analysis related to iron-binding and glycerol metabolism. This result prompted us to investigate whether the metabolites might increase or decrease with regard to their maximum rate of production and consumption (turnover) in LPM medium between 4 and 20 h. Metabolites were classified into one of three groups based on their change in turnover rate in LPM 4 vs 20 h: 'maintained' (i.e. effectively no change), 'increased' turnover in LPM 20 h, and 'decreased' turnover in LPM 20 h. For each metabolite group, we performed enrichment analysis using KEGG subsystem information to characterize impacted pathways (Figure 5C). The only metabolites that exhibited an increase in prioritization by this method were periplasmic and cellular melibiose (not shown).

KEGG subsystem enrichment analysis was performed to further characterize metabolites with maintained or reduced production and consumption (turnover) priority. Pathways related to lipopolysaccharide (LPS) biosynthesis were maintained at 20 h, but many pathways related to amino acid synthesis were reduced.

The broad increase in amino acid concentration between 4 and 20 h but decreased priority further prompted us to compare amino acid components incorporated into *S.* Typhimurium as biomass. Biomass is comprised of a number of macromolecular components, and the production of biomass effectively allows *Salmonella* to replicate. Modeled biomass constituents include lipids, glycogen, LPS, peptidoglycan, amino acids, and nucleotides, and their quantitative contribution to *S.* Typhimurium's mass has been reported previously.[36]. Several amino acid biomass components were implicated by thermodynamically infeasible loops[66] and therefore excluded from the analysis. The maximum production and consumption (turnover) of amino acids were all not maintained from 4 to 20 h (Figure 5D).

Interestingly, proline was the least impacted at 20 h and nearly maintained. Glutamate and alanine were the only amino acid components of biomass significantly altered by the reporter metabolite analysis ($p = 5.0 \times 10^{-03}$ and 4.2×10^{-02}, respectively). The only amino acid that was a component of biomass and exhibited a statistically significant decrease in concentration from 4 to 20 h was threonine ($p = 1.2 \times 10^{-02}$).

DISCUSSION

In this study, we characterized the metabolic profile of *S.* Typhimurium grown under conditions designed to induce the virulence program[38, 39] and confidently identified 66 metabolites in a GC-MS-based metabolomics study, representing the most comprehensive coverage of this organism's metabolome to date.

To gain mechanistic insight into the differences in metabolite abundances between growth conditions, we used a genome-scale model of *S.* Typhimurium metabolism as a platform for multi-omics data analysis. Although *S.* Typhimurium grows more slowly during log-phase in LPM than LB media, our condition-specific model suggests optimal growth in nutrient rich LB requires the simultaneous uptake of 13 nutrients (L-threonine, L-tryptophan, L-phenylalanine, L-methionine, L-tyrosine, L-leucine, L-serine, L-valine, L-lysine, L-histidine, L-arginine, L-glucose, and L-proline). In contrast, *S.* Typhimurium can consume these metabolites but is not singularly dependent on them to maintain optimal growth in LPM. If a similar robustness is also present in the host environment, it may facilitate *S.* Typhimurium virulence in two ways. First, the ability to consume a variety of metabolites may help to counter host strategies to sequester key growth substrates. Second, the ability to

both consume and produce a diverse repertoire of substrates may help to directly modulate host cell activation by providing the host cell with metabolites that inhibit activation of immune responses[42] or by metabolically draining the host cell. In support of the possibility that *S.* Typhimurium could provide the host with nutrients, endosomes contain transporters that may effectively transport metabolites to the macrophage's cytoplasm[6, 71].

The predicted secretion of putrescine in LB media by the omics-constrained models is consistent with the experimentally observed increase in intracellular putrescine levels with the change to LPM media ($p = 4.4 \times 10^{-5}$). Intracellular putrescine may provide *S.* Typhimurium with protection against osmotic stress in the intra-macrophage environment, as it has been shown to be a component of adaptation to osmotic stress modulated by magnesium in *Escherichia coli.*[72]

In addition to synthesis of putrescine, we predicted capacity for its consumption in LPM medium (Figure 4). Putrescine may be available to intracellular pathogens residing in the host environment since macrophages can synthesize polyamines by diverting arginine from the formation of nitric oxide, and macrophage intracellular putrescine concentrations increase following stimulation with LPS.[42]

Our present findings indicate that there is the potential for metabolic coupling between the host and *S.* Typhimurium, not just for the pathogen to access carbon and energy sources, but potentially for the pathogen to 1) exploit metabolites critically involved in adaptations to survival in the hostile phagocytic host environment and 2) inhibit or redirect host cell activation. Indeed, in a murine model of *L. donovani* infection, putrescine administered in the drinking water of mice was able to penetrate to the phagolysosome compartment and restore virulence to a mutant deficient in polyamine synthesis, demonstrating host-pathogen metabolic coupling.[73]

Additional observations of *S.* Typhimurium metabolism during growth in the virulence-inducing medium, align well with the intracellular metabolic capacity of macrophages determined in our previous study.[42] For example, the measured increase in macrophage cysteine levels agreed well with the predicted increase in capability of *S.* Typhimurium to consume cysteine in LPM versus LB (Figure 4) media. Further, statistically significant increases in macrophage fructose, D-sorbitol, and D-mannitol[42] suggested additional potential carbon sources available for growth. An additional evaluation of *S.* Typhimurium nutrient consumption, as performed in the top panel of Figure 4, predicted the capability to utilize all three in LPM medium (data not shown).

In the context of virulence, the observed alterations in the turnover flux for metabolites involved in fatty acid and proteoglycan synthesis (Supplemental Table S4) are interesting. Notably, *S.* Typhimurium is still in log phase growth at these time points. These pathways mediate adaptations to cellular membrane components, but may have further influences on adapting to a role as an intracellular pathogen. For example, peptidoglycan recycling has been reported to facilitate survival in the phagosome environment and influence host activation.[74] The control of surface modification was continued in LPM 20 h, when LPS and fatty acid synthesis pathways were among the few with maintained prioritization (Figure 5C). LPS remodeling has previously been demonstrated to both promote survival[75] and modulate macrophage activation.[76]

Acquisition of metabolic building blocks by a pathogen residing within a host is a complex interplay between the two, influenced by host sequestration of nutrients, such as iron,[77] and the pathogen's ability to adapt to the available nutrient sources within the host.[78] LPM medium approximates some of the conditions known to exist in the hostile intracellular environment, including limitation of iron, amino acid starvation, and low pH. *S.*

Typhimurium responds to these signals in specific ways, including upregulation of factors related to virulence and survival in the host, as detected in our previously published proteomics analyses of cells upon transition from LB to LPM media at 4 h (Figure 6A).[79] Interestingly, we report here an increase in intracellular amino acids in LPM medium, particularly at the 20-h time point (Figure 1), consistent with a previous report that *de novo* synthesis of amino acids occurs in *S.* Typhimurium grown intracellularly.[63] The intracellular amino acids were not among the most strongly altered metabolites based on transcriptional changes and assessed by a reporter metabolites analysis (Figure 5B). However, many amino acids, such as those involved in biomass synthesis, were observed to exhibit a decrease in priority by a consideration of the potential impact of metabolic gene expression on their production and consumption (turnover, Figure 5D), and this decrease in prioritization was apparent also at the subsystems level (Figure 5C). Our results suggested that the accumulation of amino acids was concomitant with decreases in cellular demand and supply.

Therefore, we analyzed our previously published[79] proteomics data obtained from *S.* Typhimurium grown under identical conditions to determine if proteins related to amino acid and protein synthesis were significantly ($p < 0.05$ following unpaired t-test with Bonferroni correction) altered in LPM medium between 4 and 20 h. At the 4-h time point, abundances of proteins integral to amino acid biosynthetic pathways were higher, suggesting that the initial transition to the nutrient-poor LPM environment stimulates these anabolic pathways (Figure 6B). However, the transition to stationary phase growth coincided with a decrease in protein synthesis in LPM at 20 h, as evidenced by a decreasing trend for ribosomal proteins. In addition, the abundances of tRNA synthetases and translation elongation factors were decreased, suggesting translation was diminished (Figure 6C). Taken together, these proteomics data suggest that increased amino acid production at 4 h, combined with a slowing of cell growth and protein synthesis at 20 h, contribute to the observed accumulation of amino acids within *S.* Typhimurium in LPM medium.

In summary, the analysis of metabolomics data from *S.* Typhimurium grown in rich and minimal media in the context of a genome-scale model demonstrate a potential new mechanism to disrupt immunity in the host. Further, *S.* Typhimurium may sequester amino acids during later simulated intracellular growth, perhaps in order to support rapid outgrowth during the last phases of infection.

Supplementary Material

Refer to Web version on PubMed Central for supplementary material.

Acknowledgments

This work was funded by the National Institute of Allergy and Infectious Diseases under Interagency agreement Y1-AI-8401. DRH is supported in part by a Seed Award from the San Diego Center for Systems Biology funded by NIH/NIGMS (GM085764). Significant portions of the work were performed at the Environmental Molecular Sciences Laboratory, a national scientific user facility sponsored by the Department of Energy's (DOE) Office of Biological and Environmental Research and located at Pacific Northwest National Laboratory (PNNL) in Richland, Washington. PNNL is a multi-program national laboratory operated by Battelle for the DOE under Contract DE-AC05-76RLO 1830.

References

1. Heaton JC, Jones K. J Appl Microbiol. 2008; 104:613–626. [PubMed: 17927745]
2. Voetsch AC, Van Gilder TJ, Angulo FJ, Farley MM, Shallow S, Marcus R, Cieslak PR, Deneen VC, Tauxe RV. ftEIPFW Group. Clin Infect Dis. 2004; 38:S127–S134. [PubMed: 15095181]
3. Gould LP, Nisler AM, Herman KM, Cole DDVMP, Williams IP, Mahon BM, Griffin PM, Hall AD. MMWR Morb Mortal Wkly Rep. 2011; 60:1197. [PubMed: 21900873]

4. Whitehead RN, Overton TW, Kemp CL, Webber MA. PLoS ONE. 2011; 6:e22833. [PubMed: 21829527]
5. Sun S, Berg OG, Roth JR, Andersson DI. Genetics. 2009; 182:1183–1195. [PubMed: 19474201]
6. Bumann D. Curr Opin Microbiol. 2009; 12:559–567. [PubMed: 19744878]
7. Aderem A, Adkins JN, Ansong C, Galagan J, Kaiser S, Korth MJ, Law GL, McDermott JG, Proll SC, Rosenberger C, Schoolnik G, Katze MG. MBio. 2011; 2:e00325–00310. [PubMed: 21285433]
8. McDermott JE, Yoon H, Nakayasu ES, Metz TO, Hyduke DR, Kidwai AS, Palsson BO, Adkins JN, Heffron F. Front Microbiol. 2011; 2:121. [PubMed: 21687430]
9. Buckner MM, Croxen M, Arena ET, Finlay B. Virulence. 2011:2.
10. Blank K, Hensel M, Gerlach RG. PLoS ONE. 2011; 6:e15763. [PubMed: 21264289]
11. Khoo S, Petillo D, Parida M, Tan A, Resau J, Obaro S. BMC Infect Dis. 2011; 11:241. [PubMed: 21914192]
12. Jenner RG, Young RA. Nat Rev Micro. 2005; 3:281–294.
13. Thompson A, Rowley G, Alston M, Danino V, Hinton JCD. Curr Opin Microbiol. 2006; 9:109–116. [PubMed: 16413221]
14. Yoon H, McDermott JE, Porwollik S, McClelland M, Heffron F. PLoS Pathog. 2009; 5:e1000306. [PubMed: 19229334]
15. Ramachandran VK, Shearer N, Jacob JJ, Sharma CM, Thompson A. BMC Genomics. 2012; 13:25. [PubMed: 22251276]
16. Eakley NM, Bochsler PN, Gopal Reddy P, Chopra AK, Fadl AA. Microbiol Immunol. 2011; 55:830–840. [PubMed: 22004521]
17. Mariscotti JF, Garcia-del Portillo F. J Bacteriol. 2009; 191:1855–1867. [PubMed: 19124574]
18. Shi L, Adkins JN, Coleman JR, Schepmoes AA, Dohnkova A, Mottaz HM, Norbeck AD, Purvine SO, Manes NP, Smallwood HS, Wang H, Forbes J, Gros P, Uzzau S, Rodland KD, Heffron F, Smith RD, Squier TC. J Biol Chem. 2006; 281:29131–29140. [PubMed: 16893888]
19. Adkins JN, Mottaz HM, Norbeck AD, Gustin JK, Rue J, Clauss TRW, Purvine SO, Rodland KD, Heffron F, Smith RD. Mol Cell Proteomics. 2006; 5:1450–1461. [PubMed: 16684765]
20. Vogels MW, van Balkom BWM, Heck AJR, de Haan CAM, Rottier PJM, Batenburg JJ, Kaloyanova DV, Helms JB. Proteomics. 2011; 11:4477–4491. [PubMed: 21919203]
21. Auweter SD, Bhavsar AP, de Hoog CL, Li Y, Chan YA, van der Heijden J, Lowden MJ, Coombes BK, Rogers LD, Stoynov N, Foster LJ, Finlay BB. J Biol Chem. 2011; 286:24023–24035. [PubMed: 21566117]
22. Yu JL, Guo L. J Proteome Res. 2011; 10:2992–3002. [PubMed: 21563813]
23. Sherry AE, Inglis NF, Stevenson A, Fraser-Pitt D, Everest P, Smith DG, Roberts M. Proteomics. 2011; 11:361–370. [PubMed: 21268266]
24. Haneda T, Sugimoto M, Yoshida-Ohta Y, Kodera Y, Oh-Ishi M, Maeda T, Shimizu-Izumi S, Miki T, Kumagai Y, Danbara H, Okada N. BMC Microbiol. 2010; 10:324. [PubMed: 21176126]
25. White AP, Weljie AM, Apel D, Zhang P, Shaykhutdinov R, Vogel HJ, Surette MG. PLoS ONE. 2010; 5:e11814. [PubMed: 20676398]
26. Antunes LCM, Arena ET, Menendez A, Han J, Ferreira RBR, Buckner MMC, Lolic P, Madilao LL, Bohlmann J, Borchers CH, Finlay BB. Infect Immun. 2011; 79:1759–1769. [PubMed: 21321075]
27. Antunes LCM, Andersen SK, Menendez A, Arena ET, Han J, Ferreira RBR, Borchers CH, Finlay BB. J Bacteriol. 2011; 193:4719–4725. [PubMed: 21764918]
28. Koek M, Jellema R, van der Greef J, Tas A, Hankemeier T. Metabolomics. 2011; 7:307–328. [PubMed: 21949491]
29. Cevallos-Cevallos JM, Danyluk MD, Reyes-De-Corcuera JI. J Food Sci. 2011; 76:M238–246. [PubMed: 22417363]
30. Xu Y, Cheung W, Winder CL, Goodacre R. Anal Bioanal Chem. 2010; 397:2439–2449. [PubMed: 20473487]
31. Xu Y, Cheung W, Winder CL, Dunn WB, Goodacre R. Analyst. 2011; 136:508–514. [PubMed: 21113559]

32. Zhu J, Bean HD, Kuo YM, Hill JE. J Clin Microbiol. 2010; 48:4426–4431. [PubMed: 20962140]
33. Hyduke DR, Lewis NE, Palsson BO. Mol Biosyst. 2012
34. Oberhardt MA, Goldberg JB, Hogardt M, Papin JA. J Bacteriol. 2010; 192:5534–5548. [PubMed: 20709898]
35. Thiele I, Hyduke DR, Steeb B, Fankam G, Allen DK, Bazzani S, Charusanti P, Chen FC, Fleming RM, Hsiung CA, De Keersmaecker SC, Liao YC, Marchal K, Mo ML, Ozdemir E, Raghunathan A, Reed JL, Shin SI, Sigurbjornsdottir S, Steinmann J, Sudarsan S, Swainston N, Thijs IM, Zengler K, Palsson BO, Adkins JN, Bumann D. BMC Syst Biol. 2011; 5:8. [PubMed: 21244678]
36. Raghunathan A, Reed J, Shin S, Palsson B, Daefler S. BMC Syst Biol. 2009; 3:38. [PubMed: 19356237]
37. AbuOun M, Suthers PF, Jones GI, Carter BR, Saunders MP, Maranas CD, Woodward MJ, Anjum MF. J Biol Chem. 2009; 284:29480–29488. [PubMed: 19690172]
38. Niemann GS, Brown RN, Gustin JK, Stufkens A, Shaikh-Kidwai AS, Li J, McDermott JE, Brewer HM, Schepmoes A, Smith RD, Adkins JN, Heffron F. Infect Immun. 2011; 79:33–43. [PubMed: 20974834]
39. Brown RN, Sanford JA, Park JH, Deatherage BL, Champion BL, Smith RD, Heffron F, Adkins JN. Int J Proteomics. 2012; 2012:123076. [PubMed: 22900174]
40. Coombes BK, Brown NF, Valdez Y, Brumell JH, Finlay BB. J Biol Chem. 2004; 279:49804–49815. [PubMed: 15383528]
41. Manes NP, Gustin JK, Rue J, Mottaz HM, Purvine SO, Norbeck AD, Monroe ME, Zimmer JSD, Metz TO, Adkins JN, Smith RD, Heffron F. Mol Cell Proteomics. 2007; 6:717–727. [PubMed: 17228056]
42. Bordbar A, Mo ML, Nakayasu ES, Schrimpe-Rutledge AC, Kim YM, Metz TO, Jones MB, Frank BC, Smith RD, Peterson SN, Hyduke DR, Adkins JN, Palsson BO. Mol Syst Biol. 2012; 8:558. [PubMed: 22735334]
43. Kim YM, Metz TO, Hu Z, Wiedner SD, Kim JS, Smith RD, Morgan WF, Zhang Q. Rapid Commun Mass Spectrom. 2011; 25:2561–2564. [PubMed: 21910289]
44. Kind T, Wohlgemuth G, Lee DY, Lu Y, Palazoglu M, Shahbaz S, Fiehn O. Anal Chem. 2009; 81:10038–10048. [PubMed: 19928838]
45. Hiller K, Hangebrauk J, Jäger C, Spura J, Schreiber K, Schomburg D. Anal Chem. 2009; 81:3429–3439. [PubMed: 19358599]
46. Polpitiya AD, Qian WJ, Jaitly N, Petyuk VA, Adkins JN, Camp DG, Anderson GA, Smith RD. Bioinformatics. 2008; 24:1556–1558. [PubMed: 18453552]
47. Fiehn O, Wohlgemuth G, Scholz M, Kind T, Lee DY, Lu Y, Moon S, Nikolau B. Plant J. 2008; 53:691–704. [PubMed: 18269577]
48. Smyth, GK. Bioinformatics and Computational Biology Solutions using R and Bioconductor. Gentleman, R.; Carey, VJ.; Huber, W.; Irizarry, RA.; Dudoit, S., editors. Springer-Verlag; New York: 2005. p. 397-420.
49. Ritchie ME, Silver J, Oshlack A, Holmes M, Diyagama D, Holloway A, Smyth GK. Bioinformatics. 2007; 23:2700–2707. [PubMed: 17720982]
50. Schellenberger J, Que R, Fleming RM, Thiele I, Orth JD, Feist AM, Zielinski DC, Bordbar A, Lewis NE, Rahmanian S, Kang J, Hyduke DR, Palsson BO. Nat Protoc. 2011; 6:1290–1307. [PubMed: 21886097]
51. Feist AM, Herrgard MJ, Thiele I, Reed JL, Palsson BO. Nat Rev Microbiol. 2009; 7:129–143. [PubMed: 19116616]
52. Orth JD, Thiele I, Palsson BO. Nat Biotechnol. 2010; 28:245–248. [PubMed: 20212490]
53. Becker SA, Palsson BO. PLoS Comput Biol. 2008; 4:e1000082. [PubMed: 18483554]
54. Mahadevan R, Schilling CH. Metab Eng. 2003; 5:264–276. [PubMed: 14642354]
55. Kanehisa M, Goto S. Nucleic Acids Res. 2000; 28:27–30. [PubMed: 10592173]
56. Kanehisa M, Goto S, Sato Y, Furumichi M, Tanabe M. Nucleic Acids Res. 2012; 40:D109–114. [PubMed: 22080510]
57. Perez-Llamas C, Lopez-Bigas N. PLoS One. 2011; 6:e19541. [PubMed: 21602921]
58. Patil KR, Nielsen J. Proc Natl Acad Sci U S A. 2005; 102:2685–2689. [PubMed: 15710883]

59. Oliveira AP, Patil KR, Nielsen J. BMC Syst Biol. 2008; 2:17. [PubMed: 18261202]
60. Ihaka R, Gentleman R. J Comput Graph Stat. 1996; 5:299–314.
61. Shannon P, Markiel A, Ozier O, Baliga NS, Wang JT, Ramage D, Amin N, Schwikowski B, Ideker T. Genome Res. 2003; 13:2498–2504. [PubMed: 14597658]
62. Gotz A, Goebel W. Microbiology. 2010; 156:1176–1187. [PubMed: 20075042]
63. Gotz A, Eylert E, Eisenreich W, Goebel W. PLoS One. 2010; 5:e10586. [PubMed: 20485672]
64. Eisenreich W, Dandekar T, Heesemann J, Goebel W. Nat Rev Microbiol. 2010; 8:401–412. [PubMed: 20453875]
65. Broadhurst DI, Kell DB. Metabolomics. 2006; 2:171–196.
66. Price ND, Famili I, Beard DA, Palsson BO. Biophys J. 2002; 83:2879–2882. [PubMed: 12425318]
67. Schellenberger J, Lewis NE, Palsson BO. Biophys J. 2011; 100:544–553. [PubMed: 21281568]
68. Newsholme P, Costa Rosa LF, Newsholme EA, Curi R. Cell biochemistry and function. 1996; 14:1–10. [PubMed: 8907248]
69. Fang FC, Libby SJ, Buchmeier NA, Loewen PC, Switala J, Harwood J, Guiney DG. Proc Natl Acad Sci U S A. 1992; 89:11978–11982. [PubMed: 1465428]
70. Gulig PA, Danbara H, Guiney DG, Lax AJ, Norel F, Rhen M. Molecular microbiology. 1993; 7:825–830. [PubMed: 8483415]
71. Winchester BG. Eur J Paediatr Neurol. 2001; 5:11–19. [PubMed: 11588980]
72. Munro GF, Hercules K, Morgan J, Sauerbier W. J Biol Chem. 1972; 247:1272–1280. [PubMed: 4551516]
73. Olenyik T, Gilroy C, Ullman B. Mol Biochem Parasitol. 2010; 176:109–111. [PubMed: 21182873]
74. Folkesson A, Eriksson S, Andersson M, Park JT, Normark S. Cell Microbiol. 2005; 7:147–155. [PubMed: 15617530]
75. Ernst RK, Guina T, Miller SI. J Infect Dis. 1999; 179(Suppl 2):S326–330. [PubMed: 10081503]
76. Pastelin-Palacios R, Gil-Cruz C, Perez-Shibayama CI, Moreno-Eutimio MA, Cervantes-Barragan L, Arriaga-Pizano L, Ludewig B, Cunningham AF, Garcia-Zepeda EA, Becker I, Alpuche-Aranda C, Bonifaz L, Gunn JS, Isibasi A, Lopez-Macias C. Immunology. 133:469–481. [PubMed: 21631497]
77. Bullen JJ, Rogers HJ, Spalding PB, Ward CG. FEMS Immunol Med Microbiol. 2005; 43:325–330. [PubMed: 15708305]
78. Rohmer L, Hocquet D, Miller SI. Trends Microbiol. 2011; 19:341–348. [PubMed: 21600774]
79. Yoon H, Ansong C, McDermott JE, Gritsenko M, Smith RD, Heffron F, Adkins JN. BMC Syst Biol. 2011; 5:100. [PubMed: 21711513]

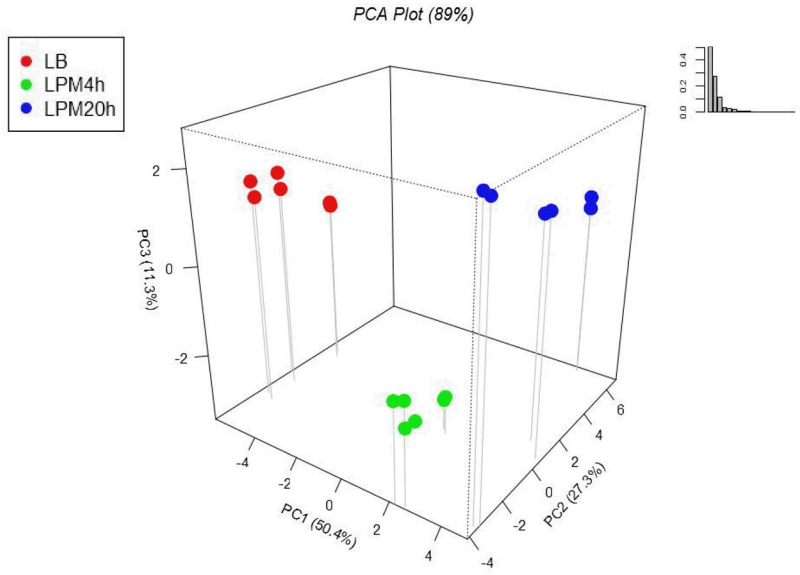

Figure 1. Principal components analysis of the curated data matrix of identified metabolites, unidentified features, and their abundances

Similarities and differences in metabolite abundances due to growth condition drove the clustering and segregation of data within and across treatment, respectively. The inset shows the variability captured by each principal component.

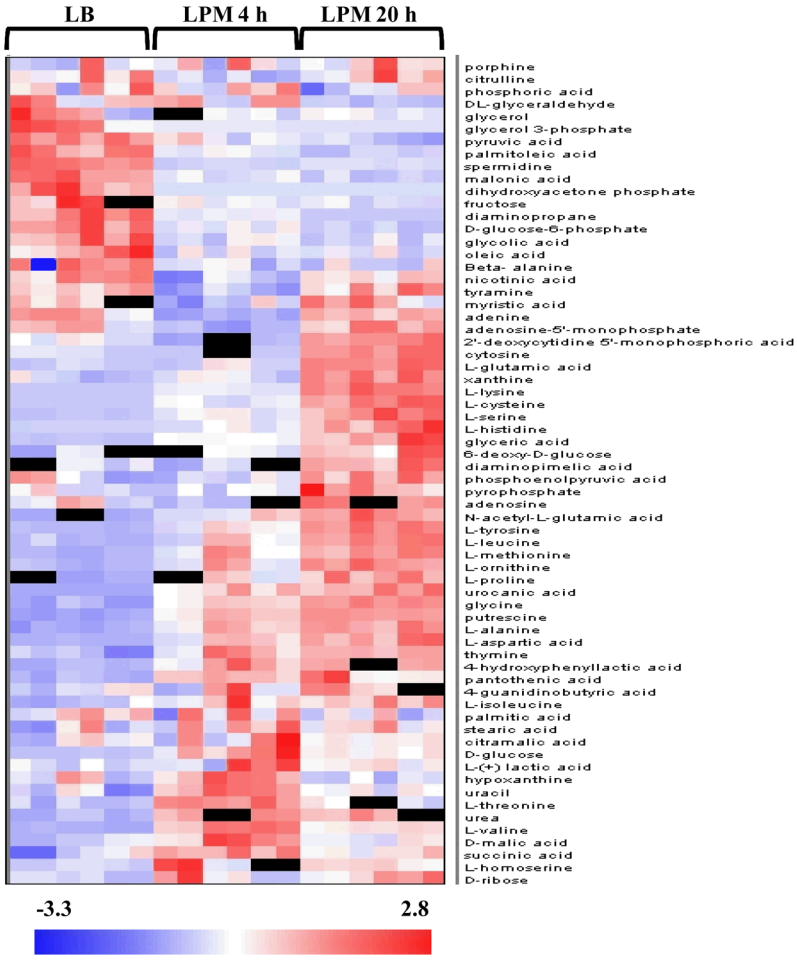

Figure 2. Heatmap of confidently identified metabolites

The abundances of 66 confidently identified metabolites were z-score transformed to facilitate data visualization and then plotted in a heat map. Each row corresponds to a unique metabolite, and each column corresponds to a technical replicate. Biological triplicates were performed and were analyzed in duplicate. Red indicates high abundance, while blue shows low abundance. Black indicates that the metabolite was not observed.

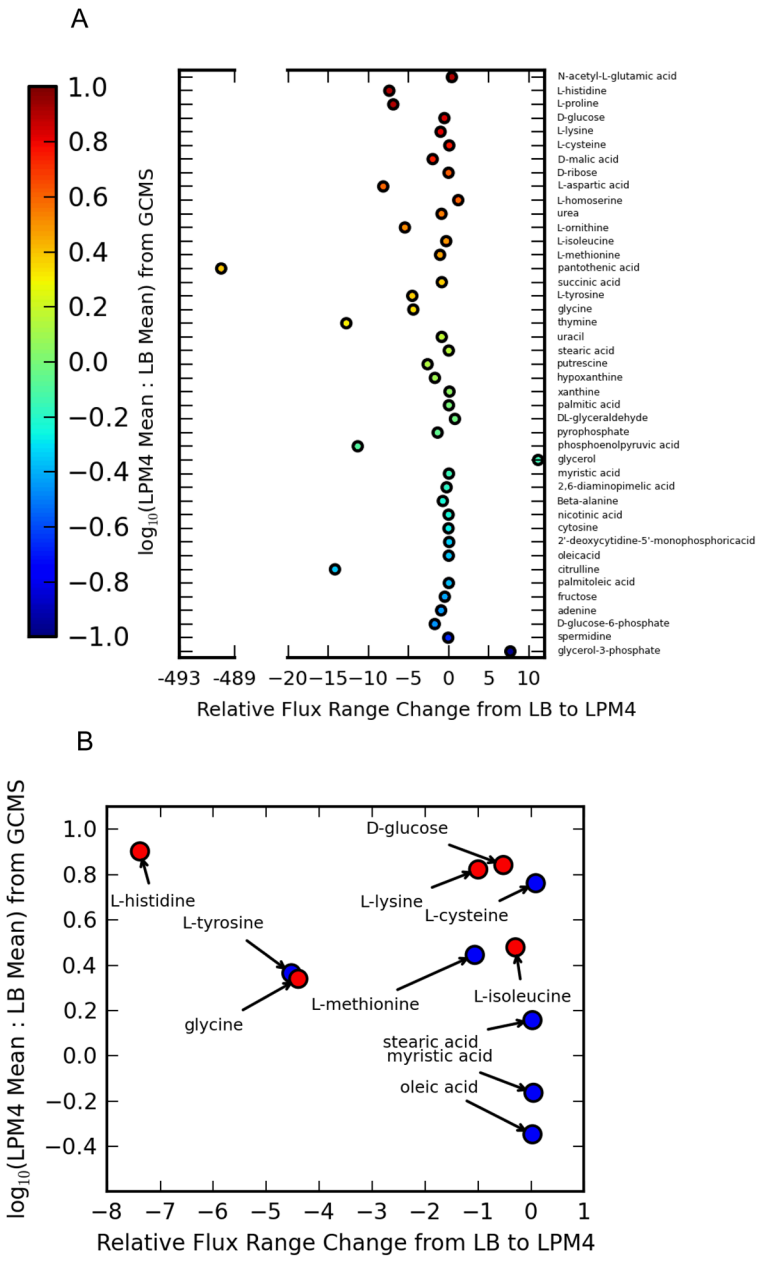

Figure 3. A comparison of concentration and relative flux range changes on the change from LB to LPM

The concentrations and relative flux range changes for all experimentally paired metabolites were compared upon the change from LB to LPM media (A). *S.* Typhimurium was in log phase growth in both conditions. Specific metabolites with putative immunomostimulatory (red) and immunoinhibitory (blue) roles were also investigated (B). The concentrations of immunostimulatory metabolites were preferentially increased in LPM relative to LB media ($p = 0.015$, red versus blue group along y-axis). Immunostimulatory metabolites exhibited a preferential relative decrease in their allowable flux range ($p = 0.060$, x-axis).

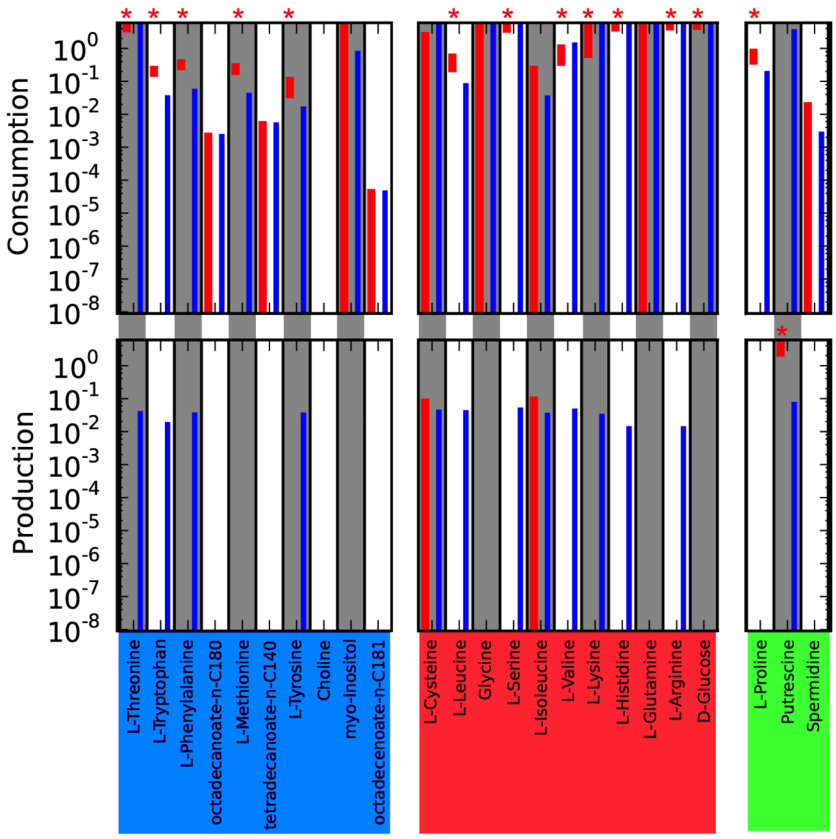

Figure 4. Evaluation of the ability of *S*. Typhimurium to consume or secrete immunomodulatory metabolites

Consumption (top frame) and secretion (bottom frame) rates for *S.* Typhimurium were evaluated, subject to limits based on metabolite solubility (maximum) and the numerical precision of the solver (minimum). The results in LB (red bars) and LPM (blue bars) media are shown. Note that the y-axis is on a logarithmic scale (mmol / g_{DW} / h). Metabolites are grouped according to classification as immunoinhibitory (blue box, bottom), immunostimulatory (pink box, bottom), or alternative macrophage activation (M2; green box, bottom). Exchanges determined to be essential for optimal *S.* Typhimurium growth in agreement with the transcriptomics data are denoted (*).

A

Model Metabolite	Compartment	Reporter *p*-value (LB-LPM 4 h)
phosphoenol-pyruvate	cytoplasm	5.5×10^{-14}
proton	cytoplasm	3.7×10^{-09}
NADP	cytoplasm	9.7×10^{-09}
NADPH	cytoplasm	1.5×10^{-08}
NAD	cytoplasm	4.3×10^{-08}
NADH	cytoplasm	5.2×10^{-08}
pyruvate	cytoplasm	7.1×10^{-08}
S-propane-1-2-diol	cytoplasm	7.3×10^{-08}
acyl-carrier-protein	cytoplasm	4.7×10^{-07}
nitrite	cytoplasm	9.7×10^{-07}

B

Model Metabolite	Compartment	Reporter *p*-value (LPM 4-20 h)
proton	periplasm	1.4×10^{-07}
proton	cytoplasm	2.3×10^{-07}
ferroxamine	periplasm	4.0×10^{-07}
ferrichrome	periplasm	4.0×10^{-07}
Fe-III-hydroxamate	periplasm	4.0×10^{-07}
coprogen	periplasm	4.0×10^{-07}
ferrioxamine-G-Fe	periplasm	4.2×10^{-07}
glycerol-3-phosphate	periplasm	1.7×10^{-06}
cytidine monophosphate	cytoplasm	2.4×10^{-06}
glycerophosphoglycerol	periplasm	1.0×10^{-05}

C

KEGG ID	Maintained Prioritization Pathway Name	*p*-value (LPM 4-20 h)
540	lipopolysaccharide biosynthesis	2.0×10^{-11}
71	fatty acid metabolism	4.4×10^{-11}
61	fatty acid biosynthesis	3.1×10^{-08}
900	terpenoid backbone biosynthesis	8.4×10^{-07}
KEGG ID	**Reduced Prioritization Pathway Name**	***p*-value (LPM 4-20 h)**
1110	biosynthesis of secondary metabolites	2.0×10^{-07}
400	phenylalanine, tyrosine and tryptophan biosynthesis	4.0×10^{-06}
340	histidine metabolism	5.9×10^{-05}
330	arginine and proline metabolism	6.7×10^{-05}
290	valine, leucine and isoleucine biosynthesis	1.1×10^{-04}
230	purine metabolism	4.1×10^{-04}
564	glycerophospholipid metabolism	9.4×10^{-04}
300	lysine biosynthesis	1.4×10^{-03}
260	glycine, serine and threonine metabolism	1.4×10^{-03}
550	peptidoglycan biosynthesis	4.9×10^{-03}
790	folate biosynthesis	8.4×10^{-03}
250	alanine, aspartate and glutamate metabolism	8.6×10^{-03}
30	pentose phosphate pathway	1.9×10^{-02}
620	pyruvate metabolism	2.0×10^{-02}
680	methane metabolism	2.0×10^{-02}
770	pantothenate and CoA biosynthesis	2.1×10^{-02}
561	glycerolipid metabolism	2.3×10^{-02}
1040	biosynthesis of unsaturated fatty acids	3.6×10^{-02}
1120	microbial metabolism in diverse environments	3.7×10^{-02}
471	D-glutamine and D-glutamate metabolism	3.8×10^{-02}
670	one carbon pool by folate	4.0×10^{-02}
270	cysteine and methionine metabolism	4.0×10^{-02}

D

Amino Acid	GC-MS ratio (LPM 20:4 h)	Reporter *p* (LPM 4-20 h)	Prioritization (LPM 4-20 h)
L-aspartate	1.6	5.1×10^{-01}	D
L-cysteine	4.7	$6.8 \times 10^{-01\#}$	D
glycine	1.4	$9.5 \times 10^{-01\#}$	D
L-histidine	5.1	8.6×10^{-02}	D
L-isoleucine	1.1	1.8×10^{-01}	D
L-lysine	5.2	$2.1 \times 10^{-01\#}$	D
L-methionine	1.4	5.5×10^{-02}	D
L-proline	1.7	5.7×10^{-01}	D
L-tyrosine	1.9	$7.7 \times 10^{-02\#}$	D
L-alanine	1.2	4.3×10^{-02}	*
L-glutamate	3.5	$5.0 \times 10^{-03\#}$	*
L-leucine	1.8	2.0×10^{-01}	*
L-serine	3.1	$3.1 \times 10^{-01\#}$	*
L-threonine	0.63	$3.4 \times 10^{-01\#}$	*

Figure 5. Exploratory, model-guided analysis of alterations in metabolism without growth as an objective

The top 10 reporter metabolites based on the structure of the metabolic reconstruction and gene expression changes between LB medium and LPM medium at 4 h (A) as well as between LPM 4 and 20 h (B) are shown. Pathway enrichment of metabolites with similar or reduced maximal turnover flux are presented and annotated as maintained or reduced prioritization, respectively (C). Comparison of GC-MS results to reporter metabolite and maximal flux ratios was performed for the amino acids utilized in biomass synthesis (D). Maintained or decreased prioritization in amino acids in LPM medium between 4 and 20 h after removing growth constraints is indicated by ‘M’ or ‘D’. Grey boxes indicate significant *p*-values using a cutoff of 0.05. Metabolites with statistically significant differences in abundance between LPM 4 h and LPM 20 h as measured by GC-MS with p values < 0.05 (see Table 2) are indicated by ‘#’. *The maximal turnover flux comparison for some

biomass components was omitted since these components are implicated by internal reaction loops.

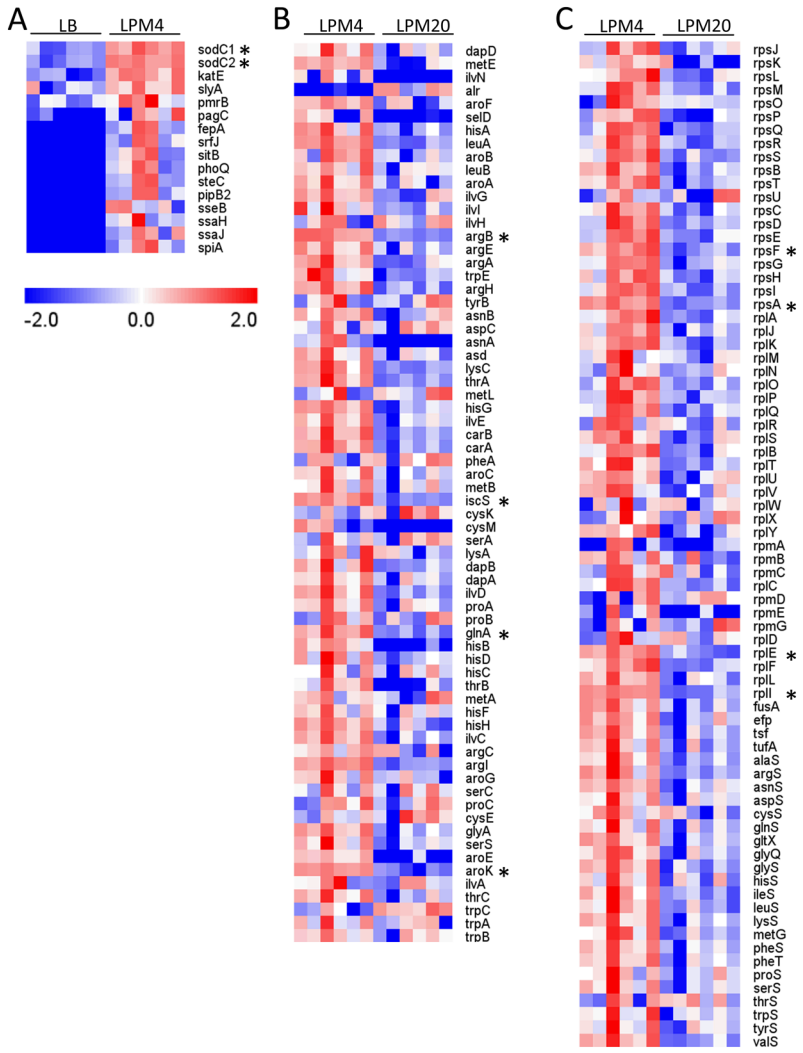

Figure 6. Accumulation of intracellular amino acids in LPM conditions is supported by complementary proteomics data

Upon transition into LPM media at 4 h, the abundances of virulence-related proteins increase (A). Proteins involved in the biosynthesis of amino acids were more abundant in LPM conditions at 4 h relative to 20 h (B). However, proteins related to translation, including ribosomal proteins, translation factors, and tRNA synthetases, were decreased during growth of *S.* Typhimurium in LPM 20 h (C). Protein abundances were considered significantly different between LPM 4 and 20 h if $p<0.05$ following an unpaired t-test and Bonferroni correction. Each row corresponds to a unique protein, and each column corresponds to a technical replicate. Biological triplicates were performed and were analyzed in duplicate.[79] Red indicates high abundance, while blue shows low abundance. Statistically significant changes are marked with (*).

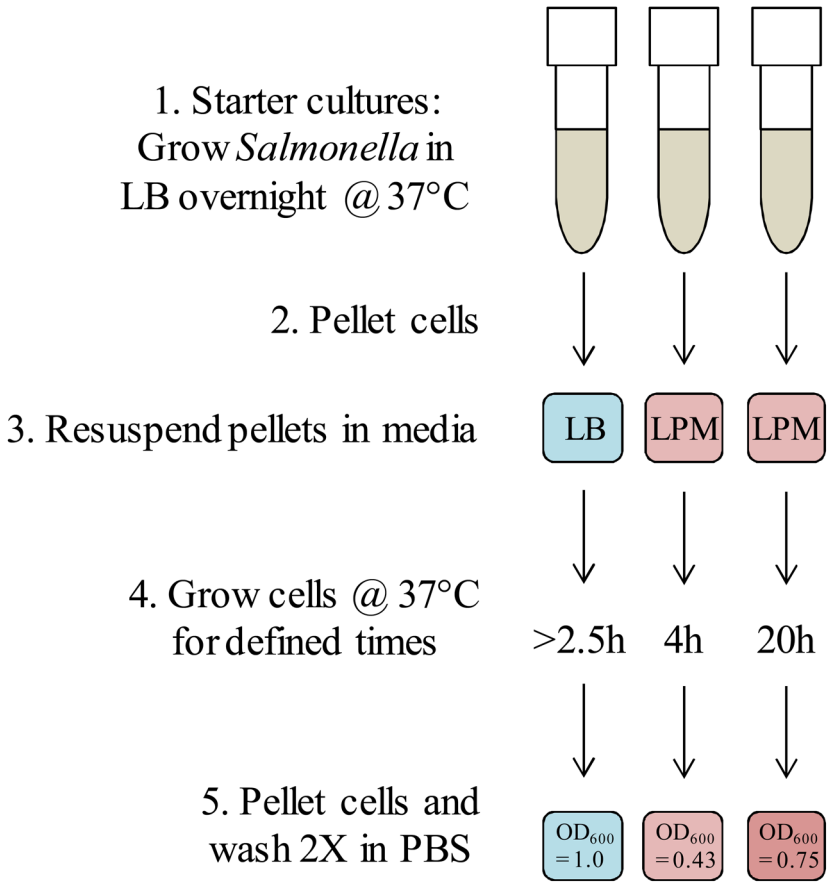

Scheme 1.

Table 1

Metabolomics coverage of the *S.* Typhimurium genome-scale model

Shown are the numbers of unique metabolites 1) identified, 2) mapped to the model, 3) unblocked, and 4) unmapped to the model for each growth condition.

	LB	LPM 4 h
Identified	65	64
Mapped to Model	59	59
Unblocked	57	57
Unmapped to Model	6	5

Table 2

Metabolites identified as having statistically significant differences in abundance among growth conditions

Metabolites with statistically significant differences in abundances between LB and LPM 4 h or LPM 4 and 20 h were determined by t-test. Bonferroni corrected *p* values < 0.05 are shown.

LB vs LPM 4 h			
Metabolite	**Bonferroni corrected *p* value**	**Metabolite**	**Bonferonni corrected *p* value**
adenine	7.8×10^{-03}	pantothenate	6.3×10^{-06}
L-alanine	5.1×10^{-03}	pyruvate	2.6×10^{-02}
L-aspartate	3.1×10^{-02}	putrescine	4.4×10^{-05}
Beta-alanine	1.7×10^{-03}	L-serine	4.9×10^{-02}
1,3-diaminopropane	9.9×10^{-03}	spermidine	9.4×10^{-07}
dihydroxyacetone phosphate	1.8×10^{-02}	L-threonine	2.8×10^{-05}
D-glucose-6-phosphate	8.5×10^{-03}	tyramine	4.3×10^{-03}
glycerate	1.3×10^{-08}	L-tyrosine	3.8×10^{-02}
glycine	2.5×10^{-04}	uracil	4.6×10^{-02}
L-lysine	1.4×10^{-04}	urea	7.8×10^{-05}
malonate	1.4×10^{-03}	urocanate	2.7×10^{-03}
nicotinate	2.1×10^{-02}	L-valine	2.2×10^{-04}
palmitoleate	4.4×10^{-03}		
LPM 4 h vs LPM 20 h			
Metabolite	**Bonferroni corrected *p* value**	**Metabolite**	**Bonferroni corrected *p* value**
adenine	1.5×10^{-06}	glycine	2.8×10^{-03}
adenosine	1.6×10^{-03}	L-glutamate	7.2×10^{-04}
AMP	1.3×10^{-03}	L-lysine	3.0×10^{-06}
L-cysteine	5.9×10^{-04}	palmitoleate	4.2×10^{-01}
cytosine	1.4×10^{-04}	phosphoenolpyruvate	1.4×10^{-02}
2′-deoxyCMP	4.4×10^{-05}	L-threonine	1.4×10^{-02}
2,6-diaminopimelate	4.9×10^{-02}	tyramine	2.2×10^{-02}
1,3-diaminopropane	2.2×10^{-07}	L-tyrosine	5.4×10^{-03}
hypoxanthine	2.9×10^{-02}	uracil	4.5×10^{-02}
glycerol 3-phosphate	4.1×10^{-05}	xanthine	2.6×10^{-03}